Modern Research in Catalysis, 2013, 2, 25-34
http://dx.doi.org/10.4236/mrc.2013.22004 Published Online April 2013 (http://www.scirp.org/journal/mrc)

Liquid Phase Hydrogenation of *p*-Chloronitrobenzene on Au-Pd/TiO_2 Catalysts: Effects of Reduction Methods

Yu-Wen Chen*, Der-Shing Lee
Department of Chemical and Materials Engineering, National Central University, Jhongli City, Chinese Taipei
Email: *ywchen@ncu.edu.tw

Received December 3, 2012; revised January 10, 2013; accepted January 19, 2013

ABSTRACT

The effects of palladium addition and the reduction methods on Au/TiO_2 were investigated. Pd was loaded on TiO_2 firstly by incipient-wetness impregnation, Au was then loaded by deposition-precipitation method. The nominal loadings of Au and Pd were 1 wt% and 0.01 wt%. The bimetallic catalysts were reduced by heating at 453 K, by flowing H_2 at 423 K, or by $NaBH_4$ at 298 K. The catalysts were characterized by ICP, XRD, TEM, HRTEM, TPR and XPS. Hydrogenation of *p*-chloronitrobenzene was carried out at 1.2 MPa H_2 pressure and 353 K. The results showed that even adding very small amount of Pd could enhance activity and selectivity of *p*-chloroaniline significantly. Pd and Au formed alloy and Pd could donate partial electron to Au. Pd metal on the surface of alloy could adsorb hydrogen and enhanced the activity. The pretreatment methods did not change particle size significantly, all were below 4 nm. The sample reduced by $NaBH_4$ could have higher concentration of Au^0 and sustain small Au particle size, resulting in high activity.

Keywords: Nanoalloy; Gold Catalyst; Au-Pd Catalysts; Hydrogenation of Chloronitrobenzene; Chloroaniline

1. Introduction

Halogenated aromatic amine is important intermediates for synthesis of organic fine chemicals, such as pesticides, herbicides, dyes, drugs and pigment, which were commercially target products. Conventional hydrogenation catalysts based on noble metal and nickel based catalyst [1-14], the noble metal such as palladium [15], platinum [16], rhodium [17] and ruthenium [18], which is limit their implementation to industrial applications because of cost effectiveness. In previous papers, one of the authors has reported that unsupported NiB catalysts are effective for hydrogenation of chloronitrobenzene [1-12].

Gold has been considered to be effective catalysts for hydrogenation reactions [19,20]. Due to its superior ability of hydrogenation adsorption, gold catalyst have many potential advantages of competitive selectivity and activity on hydrogenation reactions. The reactions included the hydrogenation of CO, CO_2, NO, ethene, propene, crotoaldehyde, citral and etc. Palladium-gold bimetallic alloys have been found to provide both active and selective catalysts for a number of reactions including CO oxidation, cyclotrimerization of acetylene to benzene, vinyl acetate synthesis, selective oxidation of alcohols to aldehydes or ketones, oxidation of hydrogen to hydrogen peroxide, and hydrocarbon hydrogenation [21]. In addition, gold-palladium alloys provide rather ideal systems for fundamental study since gold and palladium are completely miscible in all proportions with only a slight lattice mismatch [22].

Cardenas-Lizana *et al.* have investigated various catalysts for gas phase hydrogenation of *p*-chloronitrobenzene (*p*-CNB) [23-28]. It has been demonstrated that the gas phase hydrogenation of *p*-CNB over Au supported on alumina [23] and titania [24] was 100% selective in terms of $-NO_2$ group reduction to *p*-choroaniline (*p*-CAN). By investigating the influence of thin gold film surface nanostructure on chemisorption of hydrogen on unsintered gold films at 78 K, Stobinski *et al.* [29] have reported that H_2 chemisorption occurs only on Au surface atoms of low coordination number forming AuH_2 complexes. This suggests a dependence of the chemisorption process on the increasing amount of corners and edges for decreasing gold particle sizes. Since the adsorption capability of hydrogen on clean gold surface is limited, palladium was added in this study. Palladium has very strong ability to absorb up to 900 times its own volume of hy-

*Corresponding author.

drogen at room temperatures. The addition of palladium adsorbed high amount of hydrogen provides active sites for hydrogen activation. Cardenas-Lizana *et al.* [25] reported that $PdAu/Al_2O_3$ is an active and selective catalyst for vapor phase hydrogenation of *p*-CNB. The only product was *p*-CAN. High Au and Pd loadings and alumina were used in their study. In addition, the vapor phase reaction was used which is different from liquid phase reaction.

In this study, the low Au and Pd metal loadings were used, TiO_2 was used as the support instead of Al_2O_3, and the hydrogenation reaction was carried out in liquid phase. It has been reported that Au/TiO_2 was more active than Au/Al_2O_3. Therefore TiO_2 was chosen as the support in this study. In addition, it is known that the pretreatment method plays a role to determine the catalytic properties of Au, therefore the effects of pretreatment on the catalytic properties of $PdAu/TiO_2$ were also investigated.

2. Experimental

2.1. Catalyst Preparation

Pd/TiO_2 was prepared by incipient-wetness impregnation method with $Pd(NO_3)_2$ (Alfa Aesar, 99.9%) dissolved in distilled water. $Pd(NO_3)_2$ solution was added into TiO_2 (Evonik-Degussa, P25) powder in drops under slowly stirring with 0.01 wt%. It was then calcined at 300˚C for 4 h. Gold catalysts were prepared by deposition-precipitation method (DP) with 1 wt% Au nominal loading. A suspension of the support in distilled water was placed in an ultrasound bath in order to disperse the support particles. The suspension was then placed in a flask, distilled water was added and the mixture was heated to 353 K at which a solution of $HAuCl_4$ corresponding to the desired Au loading (1%, w/w), was added with a ca. 100-fold excess of NH_4OH. The pH of the suspension was adjusted to 7. The solids obtained were separated by centrifugation, washed three times with deionized water. It was dried at 353 K for 16 h.

$Au-Pd/TiO_2$ catalyst was reduced by three different ways. Catalyst was reduced either by heated at 180˚C, by H_2 gas at 423 K, or by $NaBH_4$ at ambient temperature. It is known that Au cations could be reduced by heating at 453 K. The temperature was high enough to reduce the cation, but not too high to cause sintering. $Au-Pd/TiO_2$ represents for the sample heating at 453 K. In the second method, the catalyst was heated with flowing nitrogen at 373 K for 1 h to remove water, and then reduced with 10% H_2/90% Ar gas mixture at 423 K for 2 h. In the third method, catalyst was reduced by sodium borohydride in the methanolic solution (50/50 methanol/water) at room temperature. The solution of sodium borohydride (1 M) was added into the solution very slowly under nitrogen stream to expel air in solution.

2.2. Characterization

The samples were dried under vacuum before carrying out the analysis of inductively-coupled plasma-mass spectrometry (ICP-MS), X-ray diffraction (XRD), transmission electron microscopy (TEM), high resolution transmission electron microscopy (HRTEM), energy dispersive spectrometer (EDS) and X-ray photoelectron spectroscopy (XPS).

The bulk compositions of the catalysts were analyzed by ICP-MS (PE/SCIEX Elan 6100 DRC). The ICP-MS was used for the reduction of plasma based interferences. To release mechanical stress from the inclusion, a small beam size was used to open the inclusion, followed by successive enlargement of the ablation pit. Hydrogen was used as reaction gas for the removal of plasma based interferences when operated at DRC mode. Quantitative results were calculated after calibration of the instrument response using SRM NIST 610 or 612 and a halite for Cl. Al-bulk concentrations, determined by electron microprobe, were used as internal standard in the case of the melt inclusions. The advantage from this gain in sensitivity is shown by the transient signal for a melt inclusion (40 μm diameter) from the Mole Granite. The comparison between standard and DRC operation mode shows an excellent agreement between the concentrations obtained for a series of fluid inclusions.

The XRD patterns were acquired on a Siemens D8-A powder diffractometer using Ni-filtered $CuK_{\alpha 1}$ radiation (0.15418 nm) at a voltage and current of 40 kV and 40 mA, respectively. The sample was scanned over the range $2\theta = 20^\circ - 70^\circ$ at a speed of 3˚/min to identify the crystalline structure. The samples for XRD were prepared as thin layers on a sample holder. Diffractograms were identified using the JCPDS-ICDD reference standards.

The morphologies and particle sizes of the samples were determined by transmission electron microscopy (TEM) on a JEM-2000 FX II (JEOL) operated at 120 kV and 160 kV. HRTEM was operated on a JEOL JEM-2010 at 160 kV. Initially, a small amount of sample was fed into the sample bottle filled with a 99% methanol solution. After agitating under ultrasonic environment for 90 min, one drop of the dispersed slurry was dipped onto a carbon-coated copper mesh (300#) (Ted Pella Inc., CA, USA), and dried at room temperature in vacuum overnight. Au catalysts were measured in order to obtain a good statistical particle size distribution. TEM analysis was performed using a JEOL 100 CX II microscope. The particle diameters were measured from the enlarged photographs and the particle size distribution histograms were obtained on the measurements of at least 300 ran-

domly selected individual nanoparticles. The size limit for the detection of gold particles on TiO_2 was 1 nm.

XPS spectra were recorded with a Thermo VG Scientific Sigma Prob spectrometer. The XPS patterns were collected using AlK_α radiation at a voltage and current of 20 kV and 30 mA, respectively. The sample was pressed into a self-supported disk before being mounted on a sample plate. Then it was degassed in the pretreatment chamber at 383 K for 2 h in vacuum before being transferred into the analyzing chamber. The base pressure in the analyzing chamber was maintained in the order of 2×10^{-9} torr. The spectrometer was operated at 23.5 eV pass energy. All the binding energy (BE) values were obtained after removing the surface oxides by Ar^+ sputtering and were referenced to the contaminant carbon at C_{1s} = 284.5 eV with an uncertainty of ± 0.2 eV. Peak fitting was done by using the software, XPSPEAK 4.1 with Shirley background, 30:70 Lorentzian to Gaussian convolution product shapes.

2.3. Catalytic Reaction

All the reaction experiments were carried out in a cylindrical stirred-tank reactor (Parr Instrument Model 4842). The reactor was charged by 0.002 mol Ni catalyst and 2.54 g *p*-CNB in 80 mL absolute methanol solvent, the concentration of *p*-CNB was 0.2 M. It was reported that methanol was a better reaction medium than ethanol for the hydrogenation reaction. The reactor was purged with hydrogen four times to expel air. During the run, the samples were withdrawn periodically (every 10 min) and analyzed by a gas chromatograph equipped with a flame ionization detector and a 3 m × 1/8 inch stainless steel column packed with 5% OV-101 on Chromsorb WAW-DMSC (80 - 100 mesh). Repeated catalytic runs with different samples from the same batch of catalyst delivered product compositions that were reproducible to within ± 5%. The conversion and the selectivity to each product were calculated as following:

$$C(\%) = \left[1 - \left(C_{p-CNB}\right) \Big/ \left(C_{AN} + C_{NB} + C_{p-CNB} + C_{p-CAN}\right)\right] \times 100\% \quad (1)$$

$$S_{AN}(\%) = \left[\left(C_{AN}\right) \Big/ \left(C_{AN} + C_{NB} + C_{p-CAN}\right)\right] \times 100\% \quad (2)$$

$$S_{NB}(\%) = \left[\left(C_{NB}\right) \Big/ \left(C_{AN} + C_{NB} + C_{p-CAN}\right)\right] \times 100\% \quad (3)$$

$$S_{p-CAN}(\%) = \left[\left(C_{p-CAN}\right) \Big/ \left(C_{AN} + C_{NB} + C_{p-CAN}\right)\right] \times 100\% \quad (4)$$

where C_{AN}, C_{NB}, $C_{p\text{-CAN}}$ and $C_{p\text{-CNB}}$ represented the concentration of aniline, nitrobenzene, *p*-CAN and *p*-CNB, respectively.

3. Results and Discussion

3.1. ICP-MS

The ICP-MS results shown in **Table 1** reveal the amount of exact Au and Pd loadings on the TiO_2 support. In this study, the nominal Au and Pd loadings were 1 wt% and 0.01 wt%, respectively. Only about 70% of Au and Pd were deposited on the support after DP process. The results are in agreements with literature data. Some of Pd was lost during DP process. The pretreatment did not influence the metal loadings significantly.

3.2. XRD

The XRD patterns of monometallic Au/TiO_2 catalyst and bimetallic $Au\text{-}Pd/TiO_2$ catalysts are show in **Figure 1**. All catalyst showed intense XRD peaks for antase phase at 2θ = 25.60˚(101), 38.03˚(004), 48.29˚(200), 53.94˚(105), 55.05˚(211), 62.66(204) and 68.93˚(116) and rutile phase at 2θ = 27.45˚(110), 36.09˚(101) and 54.33˚(54.33). TiO_2 from Degussa has these two phases. The preparation and pretreatment did not change the structure of TiO_2 as expected. No distinct XRD peaks for Au at 2θ = 38.2˚ and 44.5˚ were observed, because the particle size of gold was too small to detect. This confirms that Au particles were less than 4 nm. No peaks for Pd, PdO,

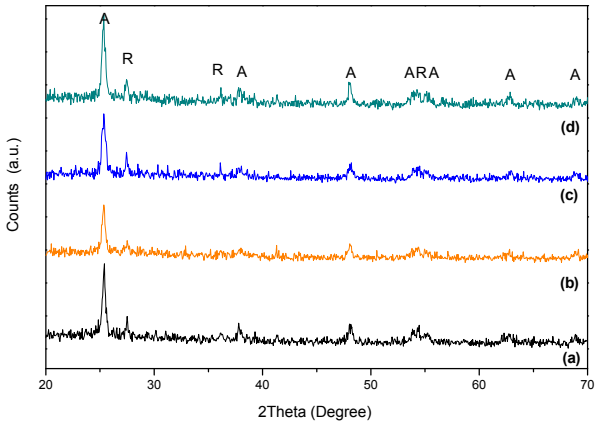

Figure 1. XRD patterns of the sample. (a) $Au\text{-}Pd/TiO_2$; (b) $Au\text{-}Pd/TiO_2$ reduced by H_2; (c) $Au\text{-}Pd/TiO_2$ reduced by $NaBH_4$; and (d) Au/TiO_2.

Table 1. Actual Au and Pd loadings of the catalysts.

Catalyst	Nominal Au loading (wt%)	Actual Au loading (wt%)	Nominal Pd loading (wt%)	Actual Pd loading (wt%)
$Au\text{-}Pd/TiO_2$	1	0.709	0.01	0.00720
$Au\text{-}Pd/TiO_2$ reduced by H_2	1	0.751	0.01	0.00774
$Au\text{-}Pd/TiO_2$ reduced by $NaBH_4$	1	0.785	0.01	0.00743

and PdO_2 were detected, which is attributed to the very low Pd loading (0.001 wt%).

3.3. TEM and HRTEM

Figure 2 shows the TEM micrographs and the corresponding gold particle size distribution of various AuPd/TiO_2 catalysts. The average Au particle size, d_{Au}, was calculated by the following equation: $d_{Au} = n_i d_i^3 / n_i d_i^2$ where n_i is the number of particles of diameter. The gold nanoparticles were homogeneously dispersed on TiO_2 support. The particle size of TiO_2 P-25 from Degussa is in the range of 20 - 40 nm. It constrained the sizes of Au and Pd particles deposited on it. **Table 2** shows that the Au-Pd/TiO_2 and Au/TiO_2 heated at 453 K had the smallest average Au particle size. Adding Pd did not change the particle size of Au because it was small enough. The sample reduced by flowing hydrogen at 423 K had slightly larger Au particles. It is known that hydrogen atmosphere and high temperature could induce migration of metal atoms. Nevertheless, the difference was very small. One can conclude that the pretreatment almost did not change the Au particle size.

Figure 3 shows the diffraction rings of Au-Pd/TiO_2 catalyst and Au-Pd/TiO_2 reduced by $NaBH_4$. The distance of lattice was calculated as follows:

$$d = 2.28034/\text{radius} \quad (1)$$

where d represents the distance of lattice, radius represents the distance from the diffraction ring or pot to the center. These two diffraction images between Au-Pd/TiO_2 heated at 453 K and Au-Pd/TiO_2 reduced by $NaBH_4$ reveal the same patterns. No palladium species was detected, which was attributed to the very low Pd loading (0.001 wt%), in consistent with the XRD results. Pd must be in very small particle size and did not form crystal itself in this study, Cardenas-Lizana *et al.* [25] have reported that Pd and Au formed nanoalloy. Our results are in accord.

The morphology, structure and orientation of the gold particles on Au-Pd/TiO_2 and Au-Pd/TiO_2 reduced by $NaBH_4$ samples have been determined by HRTEM. The HRTEM images of all Au-Pd/TiO_2 catalysts are shown in **Figure 4**. The uniform dispersion of gold particles with diameter less than 5 nm was observed. The gold particles were deposited on both rutile and anatase TiO_2. **Figure 4(a)** shows the (111) plane of gold supported on the (112) plane of the anatase phase, which neared by the (111)

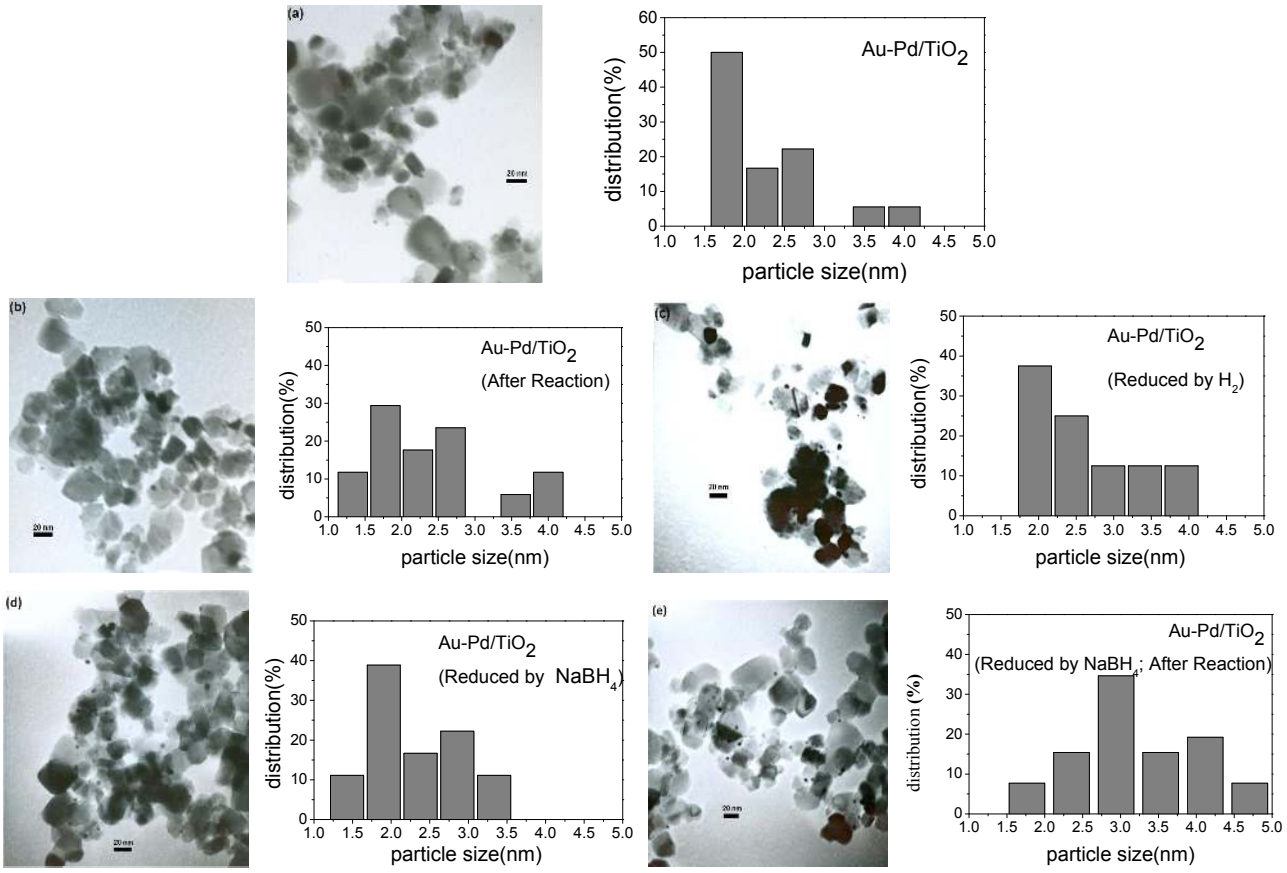

Figure 2. TEM images of the sample: (a) Au-Pd/TiO_2; (b) Au-Pd/TiO_2; (c) Au-Pd/TiO_2 (reduced by H_2); (d) Au-Pd/TiO_2 reduced by $NaBH_4$; (e) Au-Pd/TiO_2 reduced by $NaBH_4$ after reaction.

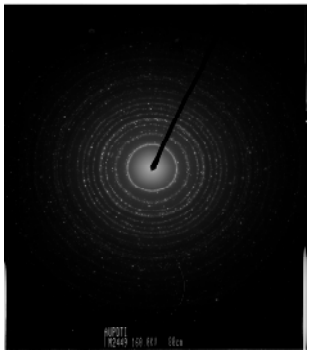

Element	Hlk	Actual distance of lattice (nm)	Nominal distance of lattice (nm)
Anatase	100	3.519428	3.52
Au	111	2.390555	2.355
Anatase	200	1.891036	1.982
Rutile	211	1.672599	1.6874
Rutile	002	1.473249	1.4797
Rutile	112	1.340734	1.3465
Anatase	215	1.257562	1.2649
Rutile	400	1.153123	1.148
Rutile	411	1.042793	1.0425

(a)

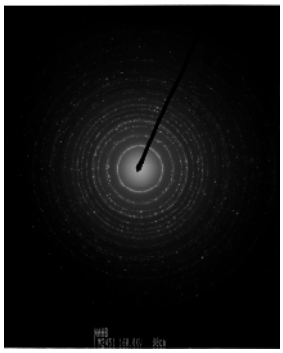

Element	Hlk	Actual distance of lattice (nm)	Nominal distance of lattice (nm)
Anatase	100	3.519428	3.52
Au	111	2.368213	2.355
Anatase	200	1.884006	1.982
Rutile	211	1.672599	1.6874
Rutile	002	1.473249	1.4797
Rutile	112	1.340734	1.3465
Anatase	215	1.254449	1.2649
Rutile	400	1.153123	1.148
Rutile	411	1.042793	1.0425

(b)

Figure 3. Diffraction ring of (a) Au-Pd/TiO_2; (b) Au-Pd/TiO_2 (reduced by $NaBH_4$).

Table 2. The average of Au particle diameter (nm).

Catalyst	Average of Au particle diameter (nm)
Au/TiO_2	2.60
Au-Pd/TiO_2	2.67
Au-Pd/TiO_2 reduced by H_2	2.99
Au-Pd/TiO_2 reduced by $NaBH_4$	2.59

plane of rutile phase of the Au-Pd/TiO_2 catalyst.

Figure 4(b) shows gold supported on the (200) plane of the rutile phase, which overlapped with the (101) plane of anatanse phase of the Au-Pd/TiO_2 reduced by $NaBH_4$. **Figure 4(c)** shows a 5 nm Au particle with (200) plane. It should be noted that no palladium species were detected, because the particle size was less than the detection limit (1 nm).

Figure 5 shows the mapping of Au-Pd/TiO_2 at the specific position on the surface of this sample. Both Au and Pd were very uniformly distributed on TiO_2 support.

3.4. XPS

The compositions and electronic structure of each species on the surface of the samples were determined by XPS analysis. The XPS spectra of Au 4f, Ti 2p and O 1s in the AuPd/TiO_2 catalysts are shown in **Figure 6**.

The de-convolution of XPS spectra for all the catalysts suggests that Au species exists in different states as metallic gold (Au^0) and Au^{3+} as shown in **Figure 6**. The Au 4f is characterized by the doublet of two spin orbit components, viz., Au $4f_{7/2}$ and Au $4f_{5/2}$. The peaks for metallic gold were centered at 84.0 eV (Au $4f_{7/2}$) and 87.7 eV (Au $4f_{5/2}$). The peaks for Au^{3+} located at 86.3 eV (Au $4f_{7/2}$) and 89.6 eV (Au $4f_{5/2}$). The Ti 2p XPS spectrum was deconvoluted into four peaks shown in **Figure 6.** The Ti $2p_{3/2}$ at 455 ± 0.3 eV is indicative of Ti^{3+}, whereas the Ti $2p_{3/2}$ at 459 eV is indicative of Ti^{4+}. The O 1s XPS spectrum was deconvoluted to two peaks as shown in **Figure 6**. The O 1s at 528 - 531 eV is indicative of metal oxides (O^{2-}), whereas that at 531 - 532 eV is indicative of hydroxides (OH^-). The deconvolution results are tabulated in **Table 3**. It should be noted that the Pd 3d signal was difficult to detect; Pd signal was very weak and overlapped with Au $4d_{5/2}$.

As shown in **Table 3**, the binding energy of Au changed with the addition of palladium and pretreatment condition. The binding energy of Au in AuPd/TiO_2 was higher than that in Au/TiO_2. The binding energy of Au shifted negatively in the AuPd/TiO_2 samples reduced by $NaBH_4$ and by H_2. One could conclude that Pd donated part electron to Au, making Au more electron-enriched.

Ti 2p did not change by adding Pd and by different pretreatments, because the pretreatment temperature was

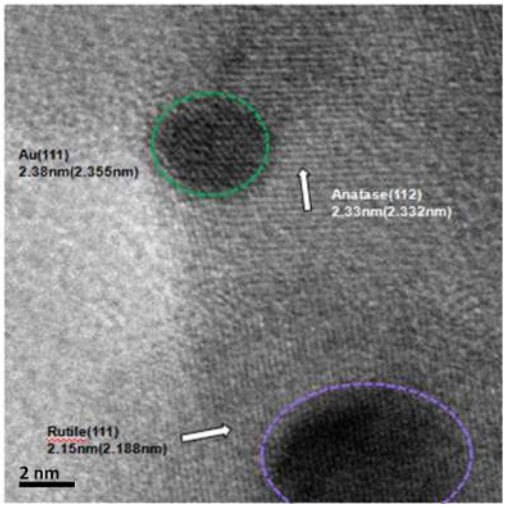

(a)

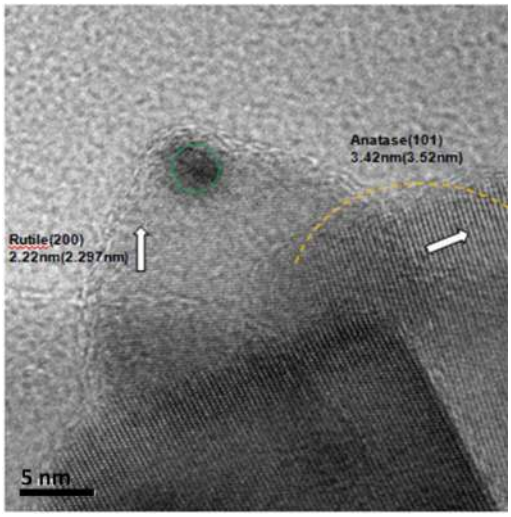

(b)

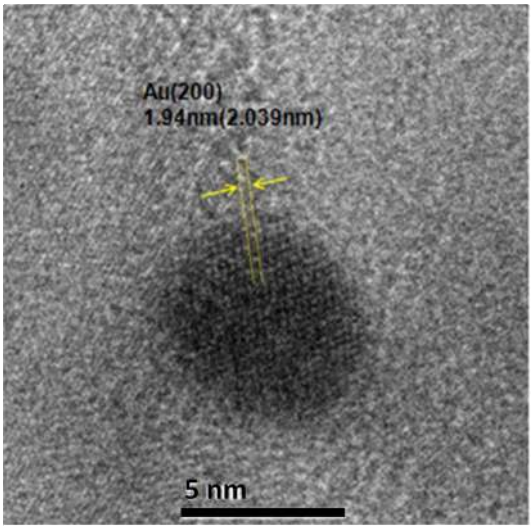

(c)

Figure 4. HRTEM image of (a) Au-Pd/TiO_2; (b) Au-Pd/TiO_2 reduced by $NaBH_4$; (c) Au-Pd/TiO_2 reduced by H_2.

not high enough to change its state. No Ti^{3+} was detected, indicating that TiO_2 structure was very stable under preparation and reduction conditions. **Table 4** shows the per-

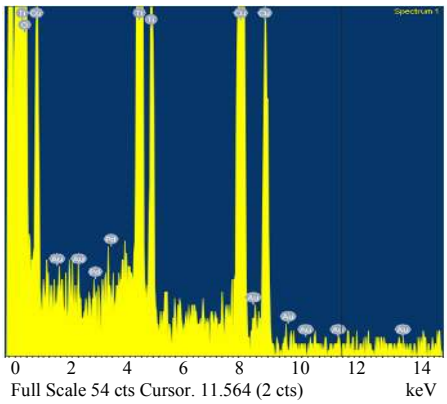

Figure 5. EDS spectra of Au-Pd/TiO_2.

Table 3. Binding energies of the species on the surface of the catalyst.

Catalysts	$Au_{4f7/2}$		$Ti_{2p3/2}$		O_{1s}	
	Au^0(eV)	Au^+(eV)	Ti^{2+}(eV)	Ti^{4+}(eV)	O^{2-}(eV)	OH^-(eV)
Au/TiO_2	84.08	-	-	458.59	530.01	531.99
Au-Pd/TiO_2	84.32	86.00	-	458.79	530.23	531.89
Au-Pd/TiO_2 reduced by H_2	83.96	85.27	-	458.66	530.12	531.94
Au-Pd/TiO_2 reduced by $NaBH_4$	83.80	-	-	458.69	530.13	531.66

Table 4. The compositions of the species on the surface of the catalyst.

Catalyst	$Au_{4f7/2}$		$Ti_{2p3/2}$		O_{1s}	
	Au^0(%)	Au^+(%)	Ti^{2+}(%)	Ti^{4+}(%)	O^{2-}(%)	OH^-(%)
Au/TiO_2	100	0	0	100	87.72	12.28
Au-Pd/TiO_2	83.97	16.03	0	100	79.42	20.58
Au-Pd/TiO_2 reduce by H_2	85.98	14.20	0	100	86.48	13.52
Au-Pd/TiO_2 reduce by $NaBH_4$	100	0	0	100	80.85	19.15

Table 5. Effect of additives on the hydrogenation of *p*-CNB over Au-Pd/TiO_2 series catalysts[a].

Catalysts	Conversion	Selectivity[b]			Reaction rate constant (s^{-1})
		p-CAN	AN	NB	
Au/TiO_2	38.23%	99.12%	0%	0.88%	0.0028
$AuPd/TiO_2$	100%	99.95%	0%	0.05%	0.0088
$AuPd/TiO_2$ reduced by H_2	77.17%	99.74%	0.19%	0.06%	0.0055
$AuPd/TiO_2$ reduced by $NaBH_4$	100%	99.17%	0%	0.83%	0.0150

[a]Reaction condition: 180 min reaction time; 1.2 MPa hydrogen pressure, 353 K, absolute methanol was medium, 500 rpm, 0.2 M *p*-CNB and 0.05 g Au catalyst. [b]*p*-CAN: *p*-chloroaniline; AN: aniline; NB: nitrobenzene.

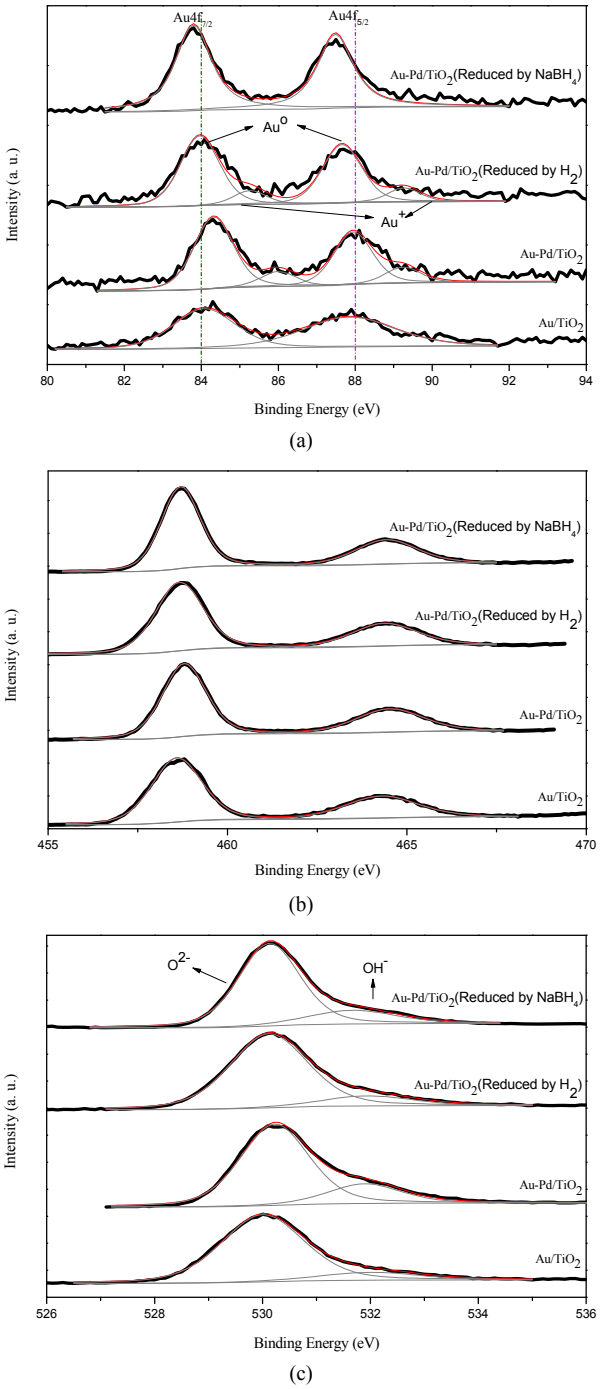

Figure 6. XPS spectra.

centages of various species on the surface of the catalysts. $AuPd/TiO_2$ reduced by $NaBH_4$ had the highest concentration of metallic Au species. It also had the highest concentration of hydroxyl groups on the surface.

3.5. Hydrogen Reaction

In order to obtain the intrinsic kinetic data, it is important to ensure that the rate data are obtained under the kinetically controlled regime. In the liquid phase hydrogenation reactions, gas-liquid, liquid-solid and intraparticle diffusion resistances are likely to be important for consumption of hydrogen. A direct test of the important of gas-liquid and liquid-solid transport was made by running the several experiments at different agitation speeds, with all other variables constant. The initial rates were found to increase significantly when the agitation speed increased from 0 to 250 rpm, but it remained constant after 300 pm. It appears from these results that the resistance to gas-liquid and liquid-solid mass transfer is not important above 300 rpm. All of the experiments were thus conducted at an agitation speed of 500 rpm. The intraparticle mass transfer in any porous solid-catalyzed reaction can be eliminated by using the small particle size <45 μm. In the present study the catalyst particle size was <30 μm and hence intraparticle mass transfer resistance was assumed to be insignificant. To confirm the absence of intraparticle mass transfer diffusion, we calculated the value of effectiveness factor. The values are close to 1 in all the experimental runs, therefore, we concluded that the intraparticle mass transfer diffusion was not significant.

Pretreatment is important for the activity of Au-Pd/TiO_2 catalyst. The pretreatment conditions should be rigorous enough to yield bare Au-Pd alloy, but not so harsh that the resulting Au-Pd particles are too large. **Figure 7** shows the conversion of *p*-CNB and selectivity of *p*-CAN vs. reaction time. It illustrates that the activity decreased in the following order: Au-Pd/TiO_2 reduced by $NaBH_4$ > Au-Pd/TiO_2 heated at 453 K ≧ Au-Pd/TiO_2 reduced by H_2 ≧ Au/TiO_2. The reaction was first-order with respect to the concentration of *p*-CNB. All the bimetallic catalysts had higher activities and selectivities than the monometallic Au/TiO_2 catalyst even only very small amount of Pd was added. The results clearly inferred that Au and Pd form alloy and had synergistic effect. Au-Pd/TiO_2 reduced by $NaBH_4$ had the highest conversion of *p*-CNB. Since *p*-CAN is the intermediate product in a series of reactions, it is expected that the selectivity of *p*-CAN is lower if the catalyst is too active. The sample heated at 453 K had smaller Au particles than that of Au-Pd/TiO_2 reduced by hydrogen. Au-Pd could be reduced by heating at 453 K. The presence of hydrogen could increase the mobility of metals, resulting in aggregation of metals. The Au-Pd/TiO_2 reduced by H_2 had the lower activity than that reduced by $NaBH_4$. The reduction temperature in flowing hydrogen was set at 423 K to avoid sintering of gold particles, but temperature might be too low to completely reduce the metal. Au-Pd/TiO_2 reduced by H_2 presented the lower conversion and selective than Au-Pd/TiO_2 reduced by $NaBH_4$ and Au-Pd/TiO_2 heat at 453 K. Proper reduction treatment of Au-Pd/TiO_2 could enhance the activity and selectivity greatly.

Since the adsorption capability of hydrogen on gold

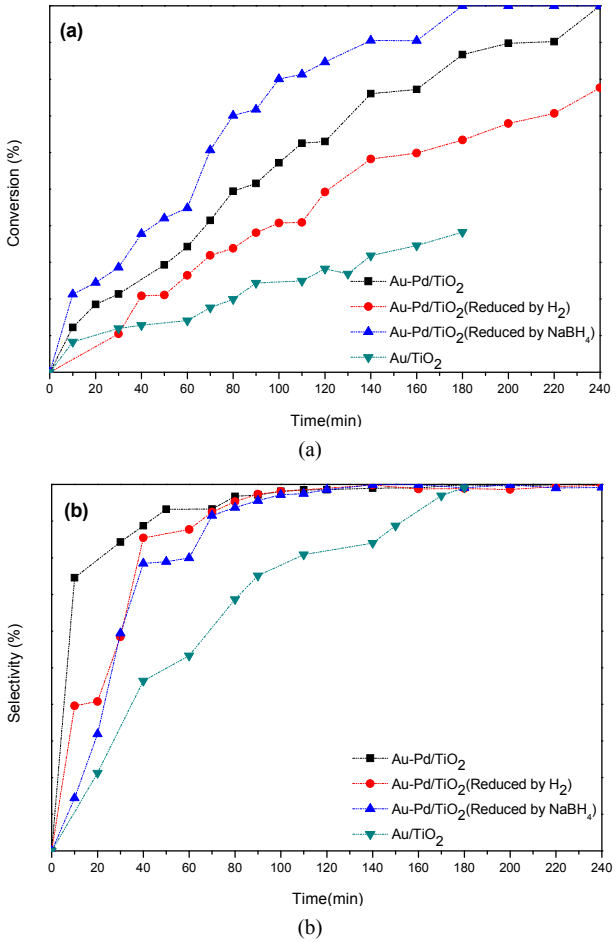

Figure 7. (a) *p*-CNB conversion and (b) *p*-CAN selectivity (Reaction condition: 0.05 g catalysts, 2.54 g of *p*-CNB, 80 ml of methanol, 353 K, H_2 pressure of 1.2 MPa, stirring speed of 500 rpm).

surface is limited [29], Pd was added in this study. Palladium has the uncommon ability to absorb up to 900 times its own volume of hydrogen at room temperatures [25]. Palladium provided active sites for hydrogen activation of Au-Pd/TiO_2 and adsorbed high amount of hydrogen. Pd donated part electron to Au which also could enhance the adsorption of hydrogen on Au. Both are beneficial for hydrogenation [25]. In the hydrogenation of *p*-CNB, since part of electron transferred from Pd to Au facilitated the catalyst attracting the partial negative oxygen easily so the N=O bond of $-NO_2$ group was activated, and the hydrogen could attack the partial positive nitrogen easily [25]. This behavior accelerated the completion of hydrogenation reaction. Combination of the electron effects and the structure effects, the Au-Pd/TiO_2 catalyst was more active after reduction by sodium borohydride rather than by H_2. The promotional effect of Pd has resulted in a significant increase in hydrogenation rate while still retaining the selectivity due to Au.

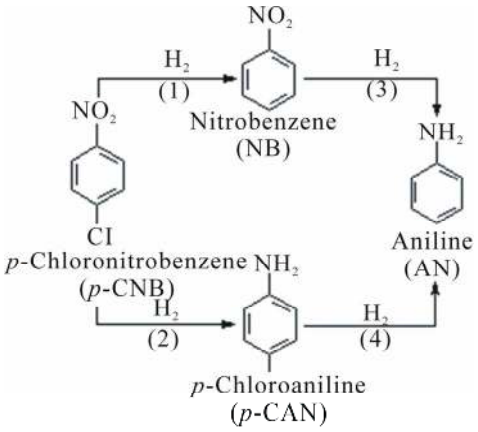

Scheme 1. Reaction mechanism of *p*-CNB hydrogenation.

In this study, the main product of *p*-CNB hydrogenation was *p*-CAN and there were two by-products, nitrobenzene (NB) and aniline (AN). The simplified reaction route is displayed in **Scheme 1**. In each case, the concentration of NB and AN increased at first, then decreased and AN would become zero eventually. There are two possible explanations: one is that *p*-CNB would mainly follow path (1) and path (2) but less to path (3) and path (4); another is that the rate of the hydrogenation carried on the path (1) is faster than the path (3). However, the increasing rate of aniline was not obvious, so the possibility of the latter case is low.

The binding energy of Au shifted to a lower value in Au-Pd/TiO_2 reduced by $NaBH_4$ catalyst, indicating that Au received more electrons from other elements. Based on the electronic effect, both $-NO_2$ and –Cl adsorb strongly on electron-rich metal, which would result in higher activity in the hydrogenation of the nitro group and de-chlorination [8-10]. Higher electron density on Au could facilitate the formation of H^- species and activating the adsorbed $-NO_2$ group through a back electron-donation from d-orbital of Au [15,16], which could promote *p*-CNB hydrogenation. It would result in strong adsorption of *p*-CNB on the active site of the elemental Au on the catalyst surface, and increased the activity of hydrogenation.

The nitro group consists of two highly electronegative elements, N and O. Oxygen atom is even more electronegative than nitrogen atom; hence, the N-O bond is polarized. The partially positive charge of nitrogen atom, combined with high electronegativity, makes the nitro-group easily reducible. The para-substituted nitro group has the high electronegativity resulting from the combination of both inductive and resonance effects. For chorine, only the inductive effect is present. Since the $-NO_2$ group is more electronegative than –Cl, $-NO_2$ is supposed to occupy the active site on the gold particles at the start of the reaction. The $-NO_2$ group adsorbed on the

catalyst surface is hydrogenated to from *p*-CAN which is further desorbed. When –Cl pre-occupied the catalyst surface, hydrogenation followed by dehalogenation occurred, leading to the formation of nitrobenzene which is eventually desorbed [30]. It is possible that the desorbed nitrobenzene would re-adsorb on the catalyst surface. As a result of the chemical bonding in the nitro group, the nitrogen atom is positively charged and each oxygen atom has a partial negative charge. For this reason the nitro group strongly attracts electrons. Since the binding energy of Au $4f_{7/2}$ was negatively shifted in Au-Pd/TiO_2 reduced by H_2, the gold on the surface became more electron-enriched. The high electronegativity of $–NO_2$ would be adsorbed on electro-rich gold, which would result in higher activity in the hydrogenation of the nitro group and dechlorination. These results establish the viability of Pd promoted selective $–NO_2$ reduction over supported Au.

The results presented here have shown that Au-Pd/TiO_2 catalyst is a promising catalyst for industrial application. The best reduction method is by sodium borohydride.

3.6. Reaction Rate Constant

One could calculate the reaction rate constant of each reaction for the monometallic Au/TiO_2 catalyst and bimetallic Au-Pd/TiO_2 catalysts. Based on the conversion-time curves in the hydrogenation of *p*-CNB (**Figure 7**), it shows that the reaction was first order with respect to the concentration of *p*-CNB. The reaction rate can be expressed as following:

$$-r_A = kC_{A0} \cdot (1 - X_A) \quad (1)$$

where k is the reaction rate constant (s^{-1}), C_{A0} is the initial concentration of reactant, and X_A is the conversion of reactant (%).

The reaction was carried out in a constant-volume batch reactor, so:

$$-r_A = C_{A0} \frac{dX_A}{dt} \quad (2)$$

where t is the reaction time (s). Combining the above two equations by using integral method of analysis of data, one could get:

$$-\ln(1 - X_A) = kt \quad (3)$$

A plot of $-\ln(1 - X_A)$ vs. t could derive the slope which represents the reaction rate constant. Because of the induction period appeared in the initial stage of reaction, the data in initial stage was neglected. The results are shown in **Table 5**. The rate constant of Au-Pd/TiO_2 reduced by $NaBH_4$ was the highest among all the samples in this study.

4. Conclusion

Bimetallic Au-Pd/TiO_2 is superior to monometallic Au/TiO_2 in selective hydrogenation of *p*-chloronitrobenzene for *p*-chloroaniline, which can be accounted for by the dominant population of the strongly bound hydrogen on Pd and the unique electronic structure of Au metal. The results showed that even adding very small amount of Pd could enhance activity and selectivity of *p*-chloroaniline significantly. Pd and Au formed alloy and Pd could donate part electron to Au. Pd metal on the surface of alloy could adsorb hydrogen and enhanced the activity. The pretreatment methods did not change particle size significantly, all were below 4 nm. The sample reduced by $NaBH_4$ could have higher concentration of Au^0 and sustain small Au particle size, resulting in high activity.

5. Acknowledgements

This research was supported by the Ministry of Economic Affairs, Taiwan.

REFERENCES

[1] Y. C. Liu and Y. W. Chen, "Hydrogenation of *p*-Chloronitrobenzene on La-promoted NiB Nanometal Catalysts," *Industrial and Engineering Chemistry Research*, Vol. 45, No. 9, 2006, pp. 2973-2980. doi:10.1021/ie0509847

[2] Y. C. Liu, C. Y. Huang and Y. W. Chen, "Hydrogenation of *p*-choloronitrobenzene Ni-B on Nanometal Catalysts," *Journal of Nanoparticle Research*, Vol. 8, No. 2, 2006, pp. 223-234. doi:10.1007/s11051-005-5944-9

[3] L. F. Chen and Y. W. Chen, "Effect of Additive (W, Mo, and Ru) on Ni-B Amorphous Alloy Catalyst in Hydrogenation of *p*-Chloronitrobenzene," *Industrial and Engineering Chemistry Research*, Vol. 45, No. 26, 2006, pp. 8866-8873. doi:10.1021/ie060751v

[4] W. J. Wang, J. H. Shen and Y. W. Chen, "Hydrogenation of *p*-Chloronitrobenzene on Ni-P-B Nanoalloy Catalysts," *Industrial and Engineering Chemistry Research*, Vol. 45, No. 26, 2006, pp. 8860-8865. doi:10.1021/ie0605736

[5] J. H. Shen and Y. W. Chen, "Catalytic Properties of Bimetallic NiCoB Nanoalloy Catalysts for Hydrogenation of *p*-Chloronitrobenzene," *Journal of Molecular Catalysis A*: *Chemical*, Vol. 273, No. 1-2, 2007, pp. 265-276. doi:10.1016/j.molcata.2007.04.015

[6] Y. W. Chen and N. Sasirekha, "Preparation of NiFeB Nanoalloy Catalysts and Its Applications in Liquid Phase Hydrogenation of *p*-Chloronitrobenzene," *Industrial and Engineering Chemistry Research*, Vol. 48, No. 13, 2009, pp. 6248-6255. doi:10.1021/ie801624a

[7] Y. W. Chen, N. Sasirekha and Y. C. Liu, "Hydrogenation of *p*-Chloronitrobenzene over NiPtB Nanoalloy Catalysts," *Journal of Non-Crystalline Solids*, Vol. 355, No. 22-23, 2009, pp. 1193-1201.

[8] M. H. Lin, B. Zhao and Y. W. Chen, "Hydrogenation of *p*-Chloronitrobenzene over Mo-modified NiCoB Nanoal-

loy Catalysts: Effect of Mo Content," *Industrial and Engineering Chemistry Research*, Vol. 48, No. 15, 2009, pp. 7037-7043. doi:10.1021/ie900019d

[9] B. Zhao and Y. W. Chen, "Hydrogenation of *p*-Chloronitrobenzene on Mo, La, Fe, and W-Modified NiCoB Nanoalloy Catalysts," *Journal of Non-Crystalline Solids*, Vol. 356, No. 18-19, 2010, pp. 839-847.

[10] B. Zhao, C. J. Chou and Y. W. Chen, "Hydrogenation of *p*-Chloronitrobenzene on Tungsten-Modified NiCoB Catalyst," *Industrial and Engineering Chemistry Research*, Vol. 49, No. 4, 2010, pp. 1669-1676. doi:10.1021/ie901606b

[11] B. Zhao and Y. W. Chen, "The Effect of Poly-N-vinylpyrrolidone Modification on NiCoB Catalysts for Hydrogenation of *p*-Chloronitrobenzene," *Materials Chemistry and Physics*, Vol. 125, No. 3, 2011, pp. 763-768. doi:10.1016/j.matchemphys.2010.09.061

[12] J. F. Su, B. Zhao and Y. W. Chen, "Hydrogenation of *p*-Chloronitrobenzene on Mo-Doped NiB Cluster Catalysts," *Industrial and Engineering Chemistry Research*, Vol. 50, No. 3, 2011, pp. 1580-1587. doi:10.1021/ie1016865

[13] Y. W. Chen and D. S. Lee, "Hydrogenation of *p*-Chloronitrobenzene on Nanosized Modified NiMoB Catalysts," *Catalysis Surveys from Asia*, Vol. 16, No. 4, 2012, pp. 198-209. doi:10.1007/s10563-012-9144-1

[14] C. P. Li, Y. W. Chen and W. J. Wang, "Nitrobenzene Hydrogenation over Aluminum Borate-supported Platinum Catalyst," *Applied Catalysis A*: *General*, Vol. 119, No. 2, 1994, pp. 185-194. doi:10.1016/0926-860X(94)85190-5

[15] R. Baltzly and A. R. Phillips, "The Catalytic Hydrogenolysis of Halogen Compounds," *Journal of American Chemical Society*, Vol. 68, No. 2, 1946, pp. 261-265. doi:10.1021/ja01206a034

[16] J. R. Kosak, "Catalytic Hydrogenation of Aromatic Halonitro Compounds," *Annals of the New York Academy of Sciences*, Vol. 172, 1970, pp. 175-186. doi:10.1111/j.1749-6632.1970.tb34975.x

[17] M. M. Dell'Anna, V. Gallo, P. Mastrorilli and G. Romanazzi, "A Recyclable Nanoparticle-Supported Rhodium Catalyst for Hydrogenation Reactions," *Molecules*, Vol. 15, No. 5, 2010, pp. 3311-3318. doi:10.3390/molecules15053311

[18] M. Liu, W. Yu, H. Liu and J. Zheng, "Preparation and Characterization of Polymer-Stabilized Ruthenium-Platinum and Ruthenium-Palladium Bimetallic Colloids and Their Catalytic Properties for Hydrogenation of *o*-Chloronitrobenzene," *Journal of Colloid and Interface Science*, Vol. 214, No. 2, 1999, pp. 231-240. doi:10.1006/jcis.1999.6186

[19] P. A. Sermon, G. C. Bond and P. B. Wells, "Hydrogenation of Alkenes over Supported Gold," *Journal of the Chemical Society, Faraday Transactions* 1: *Physical Chemistry in Condensed Phases*, Vol. 75, 1979, pp. 385-392. doi:10.1039/f19797500385

[20] R. S. Yolles, B. J. Wood and H. Wise, "Hydrogenation of Alkenes on Gold," *Journal of Catalysis*, Vol. 21, No. 1, 1971, pp. 66-72. doi:10.1016/0021-9517(71)90121-7

[21] M. Haruta, "Gold as a Novel Catalyst in the 21st Century: Preparation, Working Mechanism and Application," *Gold Bulletin*, Vol. 37, No. 1-2, 2004, pp. 27-54. doi:10.1007/BF03215514

[22] Z. Li, F. Gao, Y. Wang, F. Calaza, L. Burkholder and W. T. Tysoe, "Formation and Characterization of Au/Pd Surface Alloys on Pd(111)," *Surface Science*, Vol. 601, No. 8, 2007, pp. 1898-1908. doi:10.1016/j.susc.2007.02.028

[23] F. Cárdenas-Lizana, S. Gómez-Quero and M. A. Keane, "Ultra-selective Gas Phase Catalytic Hydrogenation of Aromatic Nitro Compounds over Au/Al_2O_3," *Catalysis Communications*, Vol. 9, No. 3, 2008, pp. 475-482. doi:10.1016/j.catcom.2007.07.032

[24] F. Cárdenas-Lizana, S. Gómez-Quero and M. A. Keane, "Exclusive Production of Chloroaniline from Chloronitrobenzene over Au/TiO_2 and Au/Al_2O_3," *Sustainable Chemistry & Green Chemistry*, Vol. 1, No. 3, 2008, pp. 215-223. doi:10.1002/cssc.200700105

[25] F. Cardenas-Lizana, S. Gomez-Quero, A. Hugon, L. Delannoy, C. Louis and M. A. Keane, "Pd-Promoted Selective Gas Phase Hydrogenation of *p*-Chloronitrobenzene over Alumina Supported Au," *Journal of Catalysis*, Vol. 262, No. 2, 2009, pp. 235-243. doi:10.1016/j.jcat.2008.12.019

[26] F. Cardenas-Lizana, S. Gomez-Quero and M. A. Keane, "Gas Phase Hydrogenation of *m*-Dinitrobenzene over Alumina Supported Au and Au-Ni Alloy," *Catalysis Letters*, Vol. 127, No. 1-2, 2009, pp. 25-32. doi:10.1007/s10562-008-9660-9

[27] F. Cardenas-Lizana, S. Gomez-Quero, N. Perret and M. A. Keane, "Support Effects in the Selective Gas Phase Hydrogenation of *p*-Chloronitrobenzene over Gold," *Gold Bulletin*, Vol. 42, No. 2, 2009, pp. 124-132. doi:10.1007/BF03214922

[28] F. Cardenas-Lizana, S. Gomez-Quero and M. A. Keane, "Clean Production of Chloroanilines by Selective Gas Phase Hydrogenation over Supported Ni Catalyst," *Applied Catalysis A*: *General*, Vol. 334, No. 1-2, 2008, pp. 199-206. doi:10.1016/j.apcata.2007.10.007

[29] C. Y. Wang, C. Y. Liu, X. Zheng, J. Chen and T. Shen, "The Surface Chemistry of Hybrid Nanometer-Sized Particles: I. Photochemical Deposition of Gold on Ultrafine TiO_2 Particles," *Colloids and Surfaces A*: *Physicochemical and Engineering Aspects*, Vol. 131, No. 1-3, 1998, pp. 271-280. doi:10.1016/S0927-7757(97)00086-1

[30] Z. K. Yu, S. J. Liao, Y. Xu, B. Yang and D. R. Yu, "Hydrogenation of Nitroaromatics by Polymer-Anchored Bimetallic Palladium-Ruthenium and Palladium-Platinum Catalysts under Mild Conditions," *Journal of Molecular Catalysis A*: *Chemical*, Vol. 120, No. 1-3, 1997, pp. 247-253. doi:10.1016/S1381-1169(96)00420-7

